NASA TECHNICAL MEMORANDUM

NASA TM X-52179

NASA TM X-52179

INCIPIENCE, GROWTH, AND DETACHMENT OF BOILING BUBBLES IN SATURATED WATER FROM ARTIFICIAL NUCLEATION SITES OF KNOWN GEOMETRY AND SIZE

by John R. Howell and Robert Siegel
Lewis Research Center
Cleveland, Ohio

TECHNICAL PAPER proposed for presentation at
Third International Heat Transfer Conference
Chicago, Illinois, August 8-12, 1966

NATIONAL AERONAUTICS AND SPACE ADMINISTRATION · WASHINGTON, D.C. · 1966

INCIPIENCE, GROWTH, AND DETACHMENT OF BOILING BUBBLES IN SATURATED WATER FROM ARTIFICIAL NUCLEATION SITES OF KNOWN GEOMETRY AND SIZE

by John R. Howell and Robert Siegel

Lewis Research Center
Cleveland, Ohio

TECHNICAL PAPER proposed for presentation at

Third International Heat Transfer Conference
Chicago, Illinois, August 8-12, 1966

NATIONAL AERONAUTICS AND SPACE ADMINISTRATION

AIChE

E-3189

INCIPIENCE, GROWTH, AND DETACHMENT OF BOILING BUBBLES IN SATURATED WATER FROM ARTIFICIAL NUCLEATION SITES OF KNOWN GEOMETRY AND SIZE

by John R. Howell and Robert Siegel

Lewis Research Center
National Aeronautics and Space Administration
Cleveland, Ohio

ABSTRACT

Artificial nucleation sites were drilled in a polished metal surface. The formation of boiling bubbles was studied by electrically heating the surface in saturated distilled water and obtaining surface temperature, heat flux, and photographic data. The surface temperature elevation above saturation required to produce ebullition is given as a function of site radius and compared with three available analyses. Data giving bubble growth as a function of site radius and surface temperature elevation is provided and compared with theoretical growth relations. At bubble detachment the buoyancy and surface tension forces are found to be in good agreement.

AUSZUG

An Hand von in eine polierte Metall Oberfläche gebohrten Löchern von bekannter Geometrie und Grösse wurde die Formierung von Dampfblasen studiert. Durch elektrisches Heizen der Oberfläche in gesättigtem distillierten Wasser wurden Temperatur- und Wärmeflussverhältnisse sowie Photographien erhalten. Der zur Aufwallung erforderliche Oberflächentemperaturanstieg über den Sättigungspunkt hinaus wird in Abhängigkeit vom Lochradius und im Vergleich mit drei vorhandenen Analysen gegeben. Die Ergebnisse für Blasenentwicklung in Abhängigkeit von Lochradius und Oberflächentemperaturanstieg werden mit theoretischen Entwicklungsbeziehungen verglichen. Im Moment des Loslösens der Blasen wurde eine gute Übereinstimmung zwischen Auftrieb und Oberflächenspannung gefunden.

АННОТАЦИЯ

На полированной поверхности металла просверленны искусственные очаги. Исследуется образование пузырей при электрическом нагреве поверхноси в дистиллированной воде и получении поверхностной температуры, потока тепла и фотографических данных.Повышение поверхностной температуры выше температуры насыщения для получения кипения приводится как функция радиуса очага и сравнивается с результатами трех имеющихся расчетов. Приведены данные изменения роста пузыря с радиусом очага и повышением поверхностной температуры. Данные сравниваются с теоретическими выражениями для роста пузырей. При отрыве пузырей силы пловучести и поверхностного натяжения находятся в хорошем согласовании.

INTRODUCTION

The boiling phenomena has been the subject of numerous research efforts, as surveyed for example in [1][1] and [2]. These investigations have revealed that many factors affect boiling, and at present there is no simple correlation that satisfactorily accounts for all the parameters involved. As a consequence, some recent research has taken the view that a quantitative understanding of the boiling problem will only be achieved by a return to very basic studies of the boiling process, starting with the formation of individual bubbles and their growth and departure. The conditions under which bubbles will be produced from a specified cavity is the principal subject of the present study.

Analytical predictions of the criteria for the initiation of bubble growth have been made [3 to 5], but only limited experimental data are available [5 to 8] relating bubble formation to a known site size and geometry, so that a satisfactory verification of these analyses has not been possible. The analyses of bubble incipience criteria by Hsu [3] and Han and Griffith [4] are quite similar. Both are based on the assumption that a surface cavity has a hemispherical vapor cap over it that serves as a bubble nucleus, and both assume that this nucleus will begin to grow only when the thermal layer of superheated liquid adjacent to the surface is of a sufficient thickness. The chief difference in the two analyses lies in the assumption of the thermal layer thickness required to produce growth for a vapor nucleus of a given height. With an assumed relation between the thermal layer thickness and the bubble nucleus size at incipience, a relation between active cavity size and surface temperature elevation is derived. The transient conduction equation is used to provide the temperature distribution in the thermal layer, and the required temperature difference for bubble growth is found from the Clausius-Clapeyron equation. For saturation conditions, Han and Griffith [4] find the maximum and minimum cavity

[1]Numbers in brackets denote references.

sizes that can be active under a constant surface temperature to be given by

$$(R_c)_{max,min} = \frac{\delta}{3}\left\{1 \pm \left[1 - \frac{12\sigma T_{sat}}{\delta\rho_v\lambda(\Delta T)_i}\right]^{1/2}\right\} \qquad (1)$$

Hsu [3] gives the relation

$$(R_c)_{max,min} = \frac{\delta}{2C_1}\left\{1 \pm \left[1 - \frac{8C_3\sigma T_{sat}}{\delta\rho_v\lambda(\Delta T)_i}\right]^{1/2}\right\} \qquad (2)$$

where the constants C_1 and C_3 are functions of the bubble-surface contact angle and the angle between the surface and the tangent to the cavity mouth. Hsu also presents an equation for the size range of active nucleation sites for the case of constant heat flux at the wall.

Griffith and Wallis [5], among others, use the Clausius-Clapeyron equation and the Gaussian expression which relates surface tension and radii of curvature to the pressure difference across the bubble interface to determine the active cavity radius. This results in the expression

$$(\Delta T)_i = \frac{2\sigma T_{sat}}{\lambda\rho_v R_c} \qquad (3)$$

In contrast with Equations (1) and (2), this relation does not indicate a maximum cavity size and predicts that only small $(\Delta T)_i$ values would be required to initiate bubbles from large cavities. The actual trend of $(\Delta T)_i$ with R_c has not been completely resolved experimentally.

Since the nucleation theories postulate that a vapor nucleus is present, they apply only to a range of cavity sizes in which vapor (or gas) is entrapped. The maximum size should thus be limited to the maximum cavity size which will not allow replacement of vapor within the cavity by the surrounding liquid. Bankoff [9] presents a method by which this size may be established for certain systems.

The present study was undertaken to experimentally determine the temperature conditions required for a cavity to become active. Because of the many parameters that could affect the system, a simple configuration was chosen, and saturation conditions were established for all tests. Yatabe and Westwater [8] noted that cavity shape appears to have little effect on nucleating characteristics, so that the only cavity parameter varied systematically was the diameter. The only system parameter varied was surface temperature (and therefore, of course, surface heat flux). In addition to cavity activation data, high-speed motion pictures were taken at and near incipience of bubble formation to study the nature of both the vapor nucleus and the bubble growth and departure characteristics from sites of known size and geometry.

APPARATUS

Heated Test Sections

The test specimens were made from number 410 stainless steel strips, 4 inches long, 1/2 inch wide, and 1/16 inch thick. The magnetic properties of this alloy allowed fine polishing on available equipment that utilized magnetic clamps. The strips were polished on all edges and on one face to a roughness less than 4 microinch rms. A 20-gage Chromel-Alumel thermocouple was then spotwelded to the center of the unfinished face of the specimen. The thermocouple leads were run parallel to the strip to reduce conduction losses. The strip was then placed in a mold which left only the finished face exposed, and epoxy resin was cast around the remaining sides providing a block of thermal insulation $4 \times 1 \times \frac{1}{2}$ inches. The artificial nucleation sites were drilled into the polished face, and the entire specimen was cleaned ultrasonically in alcohol, and finally in distilled water.

Artificial Sites

Two types of artifical sites were studied. The first type was drilled by electron-beam disintegration in the hope of producing extremely small diameters. However, the smallest site diameter attained by this method was 0.0025 inch. In addition, the disintegration tended to leave a cratered area outside the actual hole diameter. This left some doubt as to the exact geometry of the cavity. A photograph of such a cavity is shown in Figure 1(a).

The second type of artificial site was produced by a mechanical drill. This produced a hole that was quite round at the surface and with no cratering evident, (Fig. 1(b)). Diameters near a minimum of 0.003 inch were attained by this method using drills of 0.002-inch nominal diameter.

In most of the test strips, two sites of the same nominal diameter were drilled about 1 inch apart. Three strips were tested where either 4 or 6 holes of various diameters were drilled about 3/4 inch apart in a staggered pattern into the same strip, so that the effect of site diameter could be observed while all the sites were under identical conditions.

The site diameters were measured using a metallograph with a calibrated eyepiece, and the accuracy was estimated as ±0.0002 inch for mechanically drilled sites. For the electron beam sites, accuracy was about ±0.0005 inch because of the uncertainty introduced by the cratering.

Cavity depths were measured during drilling. A depth gage on the precision drill press provided this measurement for the mechanically drilled cavities, and typical values are given in Table I. The expended energy and time of disintegration were used to estimate the hole depths obtained by electron-beam disintegration. The depth-diameter ratio ranged from about 1/2 to 3 and had no effect on bubble activation.

Pool Boiler

The boiler consisted of a cylindrical stainless steel tank 14 inches in diameter and 30 inches high. Two 8-inch-diameter quartz windows were provided for viewing or photography. Four 1000-watt heaters near the bottom of the tank provided auxiliary heat to assure saturation conditions within the boiler. Two Chromel-Alumel thermocouples were immersed in the boiling water to monitor the bulk temperature. Power was provided through copper electrodes extending down through the water. The test specimen was clamped to the electrodes with the test surface horizontal. The outer surface of the boiler, including the bottom, was wrapped with 2 inches of felt insulation.

Auxiliary Equipment

Power was supplied from a motor-controlled variable output ac power transformer. The alternating current provided to the test specimen produced no problems in the temperature measuring system. Calculations based on the analysis of [10] showed that the strip geometry and physical properties were such that temperature fluctuations from the 60-cycle current were negligible.

A Fastax camera with associated timing equipment and lighting was available for photographing individual sites. Lenses and extension tubes were arranged so that the individual bubbles were magnified to practically fill the frame of the film.

Instrumentation

Test section voltage drop and current were read with 1/4-percent ac meters. The bulk water temperature and the test specimen thermocouple voltages were read with a laboratory-type potentiometer. The thermocouples were referenced to a $150^{\circ} \pm 0.25^{\circ}$ F commercial thermocouple reference oven.

PROCEDURE

The boiler tank was drained and cleaned after every second day of experimentation. An ultrasonically cleaned test specimen was clamped to the electrodes, and the boiler was charged with distilled water. The auxiliary heaters were activated until saturation was reached. To reduce the convective eddies in the tank, the power to the auxiliary heaters was decreased to a level just sufficient to maintain saturation.

Power at a low level was then applied to the specimen, and the bulk temperature, the specimen current, voltage, and thermocouple EMF readings were taken. Note was made as to the level of bubble production at the artifical site or sites (none, sporadic, intermittent, steady, etc.). The power was then increased several percent and new readings obtained. This process was continued until the artificial sites were producing bubbles continuously (except for a few cases where water evidently filled a site and no nucleation occurred). The power level was then reduced in steps of several percent each and readings taken until all activity ceased.

Photographs were taken when desired, as the tests were too numerous to permit photographs of every test condition.

The surface temperature of the specimen at which activity became steady, intermittent, or ceased with increasing or decreasing power was determined from the specimen thermocouple readings. The readings, which were taken on the back (insulated) side of the strip, were extrapolated to the boiling surface by assuming a one-dimensional heat conduction process through the specimen thickness. For a plate of thickness a, insulated on one side and having uniform internal heat generation, the temperature difference between the two sides is given by

$$T_s - T_o = \frac{qa}{2k} \qquad (4)$$

where T_o for the present experiments corresponds to the value provided by the specimen thermocouple.

RESULTS FOR BUBBLE INCIPIENCE

Definition of Incipience Point

The word incipience has been defined in a number of ways when applied to boiling. One common definition is that incipience corresponds to the surface-to-bulk temperature difference at which the ΔT versus heat flux curve begins to deviate from the free convection curve. Such a definition has little value in studying the activity of individual sites. Incipience can also be defined as the condition when the waiting time between departure and initiating a new bubble is not infinitely long. For the present experiments, however, this also has little meaning as each departing bubble left a vapor nucleus behind, and hence, the waiting time was always zero. Han and Griffith [4] and Hsu [3] in their analyses consider incipience as that temperature difference at which a given bubble nucleus begins to grow. This is a more useful criterion for the experiments reported here, but it still has some inherent difficulties. As the test section surface temperature was increased, a point was reached where a bubble would grow at the nucleation site and then remain attached to the surface. This vapor nucleus is incipient in a sense, but the condition still does not appear to be incipient boiling as a succession of bubbles is not being formed. At a slightly higher temperature level, the bubble would detach and a new bubble begin to grow, but this bubble might linger at the surface for many seconds before detaching. When the surface temperature was raised a little more, the production of bubbles became more regular. Finally, at a still larger temperature difference, a steady stream of bubbles appeared from the cavity. The question is, which of these conditions establishes incipience?

Because the irregularities in the nucleation phenomena may well be due to the statistical fluctuations inherent in the thermal boundary layer thickness, it seems that steady, or regular, activity could only occur when the thermal boundary layer thickness reached a mean value greater than that used in the incipience criteria of [3] and [4]. Fluctuations around the "incipience" or smaller thermal layer thicknesses might produce irregular activity if the ΔT value is below the "incipience" ΔT.

In the present study, it was decided to examine the incipience point with regard to two definitions. One definition that provided an upper limit was that incipience corresponds to the ΔT at which regular bubble production occurred from a given site. It is obvious that such a definition involves possible errors in the judgment of the observer and may produce $(\Delta T)_i$ values above the theoretical predictions. It also involves the experimental difficulty of defining "regular" production from sites of differing size. If a large and a small site are compared in the region of incipience, the frequency of bubble emission is lower for the larger site as this site is producing larger bubbles; however, the percentage variations around a given mean bubble frequency seemed smaller for large sites. Thus, a small site could be producing a fair number of bubbles but not be incipient according to this definition because of a lack of bubble regularity, while a large site producing at a lower frequency with bubble regularity would meet this incipience criterion.

The second definition of incipience was that it corresponds to the minimum ΔT at which bubbles grow and detach from the surface. Below this ΔT, a bubble might be present at a site, but it would

continue to remain attached to the surface. This criterion would be expected to correspond more closely with a theory based on the assumption that incipience is achieved when a nucleus will grow but with no consideration as to whether a stream of bubbles is produced. For this definition of incipience, the thermal boundary layer thickness will occasionally reach the required thickness for bubble growth and detachment.

Incipience of Nucleation

The data for the surface-to-bulk temperature difference at which steady emission occurred according to the first definition of incipience are plotted as a function of site radius R_c in Figure 2(a). The $(\Delta T)_i$ from the second definition are given in Figure 2(b). The points in Figure 2(a) are those $(\Delta T)_i$ values at which emission appeared to be steady, but for which the next step decrease of about 10 percent in heat flux caused extinction or extreme decrease of the site activity. In Figure 2(b), the $(\Delta T)_i$ were taken when a very few bubbles were being produced. Where a range is shown about a data point, the lower limit extends to where bubble detachment ceases, while the upper limit provided a few bursts of bubbles. The incipience temperatures obtained with increasing heat flux generally were higher for a given site radius, and had more scatter. These values are not shown. The fluid bulk was always maintained at the saturation temperature.

For an individual site, a statistical scatter in the emission behavior would be expected as is characteristic of boiling processes. As shown in Figure 2, the scatter was on the order of several degrees. At each site radius, the minimum $(\Delta T)_i$ may be regarded as corresponding to thermal layer conditions most favorable to bubble growth. When making comparisons with theory, the envelope through the minimum $(\Delta T)_i$ points should be kept in mind, since it delineates the boundary between the inactive region and the region of possible activity.

Comparison with Analyses of Incipience

Equations (1) to (3) each predict a $(\Delta T)_i$ versus cavity radius relation that defines a size range for active cavities. The most simple of these, (Equation (3)), has the possible shortcoming of predicting no maximum active cavity size. A plot of this equation in Figures 2(a) and (b) shows that it does lie to the left of all the data, but the $(\Delta T)_i$ values are smaller than those observed. At large site radii, the deviation increases as the data tend toward larger $(\Delta T)_i$ values in Figure 2(a), or remain fairly constant in Figure 2(b). These trends are in opposition to Equation (3), where $(\Delta T)_i$ decreases with increasing R_c.

The relation of Han and Griffith [4] as given in Equation (1), requires a knowledge of the thermal layer thickness. This has been measured by Marcus and Dropkin [11], who provide a correlation between thermal layer thickness and heat transfer coefficient. For values of heat transfer coefficient in the range of the present experiments (2×10^3 to 4×10^3 Btu/(hr)(ft^2)($^\circ$F)), an average thermal layer thickness is $\delta \approx 0.006$ inch. Using this δ, Equation (1) has been plotted in Figure 2(a), and it does not bound most of the data. Since the maximum value of Equation (1), which is found as $(\Delta T)_i \to \infty$, is $R_{c,max} = 2\delta/3 = 0.004$ inch, the relation cannot account for the larger drilled sites employed here unless the δ value were made much larger.

In addition to requiring a value of δ, Equation (2) of Hsu [3] has coefficients C_1 and C_3 that depend on the cavity geometry. If the values of C_1 and C_3 used in [3] are assumed here, a curve similar to that from Equation (1) is obtained. If the mouth of the cavity is assumed to have a perfectly square edge as an idealization of the machine-drilled sites, then C_1 and C_3 are equal to unity. With these values Equation (2) was evaluated and is shown in Figure 2(a). The curve, which strictly should be compared only with the machine-drilled data because of the choice of constants, encompasses a little more of the experimental values than the Han and Griffith relation, but it still does not extend to a sufficiently large range of active sites.

The incipience theories were founded on the assumption that for a bubble to begin to grow, the temperature in the thermal layer at a characteristic position, for example, at the top of the bubble nucleus, must reach the temperature of the vapor inside the nucleus. This type of assumption clearly cannot apply to some of the results obtained here for large cavities. For example, with a cavity radius of 0.020 inch the nucleus left by a departing bubble would be in the range of 0.010 to 0.020 inch in height, which is substantially larger than the thermal layer thickness. Hence, the assumptions in the theory would rule out the observed activity at the large sites tested.

One question is whether the thermal layer thickness of 0.006 inch used here is really correct. This is an "extrapolated" thickness obtained in [11] by extending the linear part of the temperature profile near the heated surface until the bulk temperature is reached at the distance δ. Hence, this layer does not include the region where the fluid temperature gradually decreases to the bulk value. In this region, there could be significant heat addition to the vapor nucleus.

It could be argued that the nucleation that appears to come from the large cavities is occurring at smaller nucleation sites contained within the larger sites. However, Bankoff [9] shows that rectangular grooves up to a width of 0.07 cm (0.028 in.) will retain any vapor originally trapped within them when immersed. He further states that cylindrical cavities of this ($R_c = 0.014$ in.) or perhaps slightly larger radius should also retain entrapped vapor. This fact, coupled with the high-speed motion pictures discussed in succeeding sections, which showed no liquid entering the cavities between bubbles (and, in fact, showed a vapor cap left over the site by the departing bubbles), makes this "site-within-a-site" explanation doubtful for the data presented here. It appears that some modification of the thermal-layer bubble-nucleus mechanism advanced in [3] and [4] is needed to account for the observed nucleation from large sites in saturated liquid.

Minimum Incipience Temperature

The theory in [3] predicts reasonably well both the minimum $(\Delta T)_i$ and the site radius at which it will occur for the regular activity incipience data of Figure 2(a). This tends to confirm that Equation (2) can adequately predict the minimum $(\Delta T)_i$ in a system where a large site size range exists and where the thermal layer thickness

is known. This was verified experimentally by Bergles and Rohsenow [12] for a flowing system where the thermal layer thickness is known, by using the earlier incipience analysis of Hsu and Graham [13].

Modified Incipience Criteria

For sites of such a size that their attached nuclei extend through the thermal layer, $R_c > \delta$, the model shown in Figure 3(a) can be analyzed. Heat will be added to the nucleus through that portion of the nucleus surface within the thermal layer, while condensation will occur over the remainder of the nucleus area. With the bulk temperature of the liquid at saturation, the temperature profile within the thermal layer can be approximated by the linear relation

$$T(x) - T_{sat} = (T_w - T_{sat})\left(1 - \frac{x}{\delta}\right); \qquad x \leq \delta \qquad (5)$$

If the vapor temperature within the nucleus is assumed constant and given by

$$T_v - T_{sat} = \frac{2\sigma T_{sat}}{\lambda \rho_v R_c} \qquad (6)$$

the net heat added to the nucleus is given by

$$Q = h_e 2\pi R_c \int_0^{\delta} \left[\left(T_w - T_{sat}\right)\left(1 - \frac{x}{\delta}\right) - \frac{2\sigma T_{sat}}{\lambda \rho_v R_c}\right] dx - h_c 2\pi R_c \int_{\delta}^{R_c} \left(\frac{2\sigma T_{sat}}{\lambda \rho_v R_c}\right) dx \qquad (7)$$

The quantities h_e and h_c are the evaporating and condensing heat transfer coefficients for heat transfer to the nucleus and have been assumed constant. This assumption may be open to question, as the coefficients probably depend on the thermal history of the nucleus.

For the nucleus to grow, Q must be greater than zero, leading to the criterion

$$(T_w - T_{sat})_i = (\Delta T)_i > \frac{4\sigma T_{sat}}{\lambda \rho_v \delta}; \qquad R \geq \delta \qquad (8)$$

where the heat transfer coefficient h_e has been taken equal to h_c.

If the nucleus is contained wholly within the thermal layer (Fig. 3(b)), the heat added to the nucleus is given by

$$Q = h_{e,c} 2\pi R_c \int_0^{R_c} \left[\left(T_w - T_{sat}\right)\left(1 - \frac{x}{\delta}\right) - \frac{2\sigma T_{sat}}{\lambda \rho_v R_c}\right] dx \qquad (9)$$

which, for $Q = 0$, gives

$$(\Delta T)_i = \frac{2\sigma T_{sat}}{\lambda \rho_v R_c} \cdot \frac{1}{\left(1 - \frac{R_c}{2\delta}\right)}; \qquad R_c \leq \delta \qquad (10)$$

A plot of Equations (8) and (10) is given in Figure 2(b), using $\delta = 0.006$ inch, and the theory agrees more closely with the data than do the other analyses. No maximum site size is indicated by this analysis. This indicates that heat transfer may not be the limiting process for bubble incipience from large sites, and that perhaps vapor replacement in the cavities provides the upper limit to active cavity size.

The minimum incipience temperature difference, as given by Equation (8), corresponds to 1/2 the value predicted by Hsu in Equation (18a) of [3]. This difference is due to Hsu's assumption, which relates thermal layer thickness at incipience to cavity size. The minimum $(\Delta T)_i$ predicted by Equation (8) agrees closely with the data for initial bubble growth shown in Figure 2(b).

An analysis similar to the above, except that it is based on the surface heat flux rather than the surface temperature, has been given by Grace [14].

The analysis presented here can be extended to include the effect of subcooling on the activation of individual sites, and this work will be presented in a future publication.

CHARACTERISTICS OF BUBBLES AT DRILLED SITES

Growth of Bubbles While Attached to Surface

By having mechanically drilled sites in a polished surface and by using low heat fluxes near incipience, it was possible to grow isolated bubbles that were not disturbed by adjacent bubble formation. The high-speed motion pictures showed the bubble profiles to be symmetric about the site axis, and the bubbles had little distortion.

Figure 4 shows a set of tracings for the growth of two bubbles, one for each of the mechanically drilled site diameters 0.0075 and 0.0413 inch. These sites, along with two others, were drilled into the same heated strip, and photographs were taken at the four sites in rapid succession without changing the experimental conditions, so that the heat flux and surface temperature were held constant. Hence, the pictures presumably compare the growth of bubbles under the same condition of the thermal layer on the surface. However, the random convective circulation currents in the boiler caused some fluctuations in the thermal layer thickness. This resulted in some of the bubbles at a given site having lower growth rates than others, even though the time average conditions remained fixed. This statistical variation was also noted in [7]. To make comparisons of bubbles taken at different sites, the statistical randomness was removed as much as possible. This was done by selecting the bubble at each site that had the most rapid growth rate and increased in volume continuously to detach in the shortest growth period. This should correspond most closely to the conditions for which the theoretical growth equations apply. These are the bubbles shown for two sites in Figure 4 and are presumed to be growing under thermal conditions as consistent with each other as possible.

The bubbles were assumed to be rotationally symmetric about the site axis and their volumes were computed from the profiles. For some of the bubbles near detachment, where they were not close to spherical, the width of the bubble was measured

at 15 positions along the bubble height, and the volume was computed by numerical integration. For the remainder of the bubbles, the shape could be approximated within a few percent error by a sphere or a spherical segment, and the volume was computed analytically.

The volumes are given as a function of time in Figure 5 for the growth period. Since the photographs were taken at a film speed of approximately 2000 frames per second, there is a time lapse of somewhat less than 1/2000 second between frames, since recording the image on the film requires a portion of the time. Hence, the first data point can be a maximum of a few ten thousandths of a second after the detachment of the previous bubble. If the data could be extrapolated to zero time, the initial bubble volume would not be zero, because there was always a vapor nucleus left behind by the previous bubble. The last few pictures in each set of profiles in Figure 4 illustrate how the bubble neck narrows and then breaks off, leaving a vapor nucleus behind.

Some aspects of bubble departure from a known site were studied by Wei and Preckshot [15] who photographed bubbles leaving a short section of glass capillary that had been cemented to a glass slide placed on a heated copper block. In this case (where the cavity itself was not within the heated surface), after a bubble detached, there was a small vapor pocket left at the bottom of the cavity, and the remainder of the cavity filled with liquid. The small vapor pocket grew to form the next bubble. In the present experiment, the cavity was within the heated surface and, either because of this or the cavity shape or material, the vapor nucleus was much larger than that in [15]. The vapor nucleus was always observed to protrude well above the cavity opening. For this reason, it is thought that the walls within the cavity were always dry without any liquid microlayer inside. Within the very short time after bubble departure and before the next frame showing the new bubble, the surface tension formed the nucleus into the shape of a spherical surface. For a small site (Fig. 4(a)) the nucleus was almost in the shape of a complete sphere, while for a larger site (Fig. 4(b)) it was a short spherical segment.

It is postulated here that the growth of the bubble depends on the heat addition from the thermal layer surrounding the bubble base. Hence, the bubble growth depends on how much bubble surface area is within the thermal layer. It has been assumed in analyses such as those by Zuber [16] and Han and Griffith [4] that the growing bubble nucleus pushes the thermal layer outward, so that the bubble is surrounded by the layer. As discussed previously, the thermal layer thickness for the heat fluxes encountered here was about 0.006 inch. This thickness, shown in Figure 4, is about 1/2 the height of the vapor nucleus left by the departing bubble. Hence, for the present cases, it is possible that the heat transfer to a bubble was only through the area near the base in contact with the thermal layer (area A in Fig. 6). The growth of the bubble then depends on the time variation of A. As a very simple illustration, assume that the heat transfer coefficient at the bubble base and the average temperature within the thermal layer remain constant throughout bubble growth. Then

$$hA(T_{t\ell} - T_v) = \frac{dV}{d\tau}\rho_v\lambda \qquad (11)$$

The time variation of A must be considered in order to integrate for V. From the profiles in Figure 4, after about 0.001 second the bubbles are quite close to spherical segments and are of the successive configurations shown in Figure 6(b). Area A of the spherical zone within the thermal layer is $A = \pi D\delta$. If the volume of the bubble is approximated by $V = \frac{\pi D^3}{6}$, then $A = \pi\left(\frac{6V}{\pi}\right)^{1/3}\delta$. Substituting into Equation (11) and assuming that the thermal layer temperature and thickness remain constant during bubble growth give the functional form

$$V^{1/3} \propto \frac{dV}{d\tau} \quad \text{or} \quad V \propto \tau^{3/2} \qquad (12)$$

In the later stages of growth when the bubble begins to elongate and especially when a neck begins to form, area A tends to become constant (Fig. 6(c)). Then, from Equation (11) $dV/d\tau$ is a constant. This gives

$$V \propto \tau \qquad (13)$$

This first power behavior was also observed in [17]. The trend of decreasing slope during growth of the curves in Figure 5 might then be attributed in part to the changing configuration near the bubble base. The fact that the temperature in the thermal layer $T_{t\ell}$ actually decreases during growth [18 and 19] and that the thermal layer thickness δ may also decrease during growth [13] contributes further to a reduction in growth rate.

When a bubble is formed at a very small natural nucleation site, the base does not stay attached to the site but rather expands rapidly outward at first and then remains relatively constant until detachment begins (e.g., base measurements in [17]). The rapid growth in the base diameter produces a rapid increase in the bubble area within the thermal layer, which could account for the fact that in the expression

$$D \propto \tau^n \qquad (14)$$

the n values have been as large as unity near the beginning of bubble growth [20].

To see how the present data compare with some of the commonly quoted simple models for bubble growth, two expressions have been plotted in Figure 5; the Fritz-Ende [21] expression

$$V = \frac{\pi}{6}\left(\frac{4k_\ell\Delta T}{\lambda\rho_v}\right)^3\left(\frac{\tau}{\pi\alpha}\right)^{3/2} \qquad (15)$$

and the Plessett-Zwick [22] expression

$$V = \frac{\sqrt{3}\,\pi}{2}\left(\frac{4k_\ell\Delta T}{\lambda\rho_v}\right)^3\left(\frac{\tau}{\pi\alpha}\right)^{3/2} \qquad (16)$$

For the part of the data where $V \propto \tau^{3/2}$ the Fritz-Ende result provides a reasonable prediction. This was also found in [17].

In Figure 7(a), growth curves for $D_c = 0.0075$ inch are shown for three ΔT values. The curves were again selected as having the most rapid growth. Comparison is made with the Fritz-Ende equation, and although the experimental data do not fall on the analytical lines, agreement is good regarding trends with ΔT and slopes with time.

In Figure 7(b), growth curves for bubbles at a larger site, $D_c = 0.0413$ inch, are shown. Correla-

tion with the analytical curves is obviously poorer than for the smaller site. Two possible reasons for this are evident: first, the models used in deriving the analytical expressions assume that the bubble is surrounded by superheated liquid. This is doubtful for the very large bubbles growing from the larger sites, especially during the later stages of growth. Another reason is that because of the lower frequency of bubble emission from the larger sites at a given ΔT, relatively fewer bubbles were available on each film roll for obtaining growth curves. Thus, in selecting the most rapid growth curve for each given ΔT, the probability of obtaining comparable curves for comparison between the different ΔT values was not as good as for the higher frequency small site.

Forces Acting on Bubbles at Departure

The shapes of typical bubbles formed at drilled sites are shown in Figure 8(a) just prior to the start of departure by necking down at the base. In the present experiments, it is believed that the forces on the bubble at departure can be computed very accurately. At departure, the cylindrical neck at the base of the bubble was found to stretch in length and become narrower until the neck was broken. Hence, the force holding the bubble near the surface is the surface tension of the interface around the circumference of the bubble neck. This surface tension force can be computed quite accurately, since it does not depend on the contact angle of the liquid-vapor interface at the heated surface. During boiling, this contact angle is difficult to measure. As will be shown, the diameter of the bubble neck is known accurately here, because it corresponds quite well with the diameter of the drilled site.

Another factor that contributes to the accuracy of the force balance at departure is that there is no microlayer under a bubble attached to a drilled site. For a bubble growing from a natural nucleation site, the possible presence of a fluid microlayer casts some doubt as to the correct area of the bubble base.

The buoyancy force of the bubble at departure can be computed by a method proposed in reference [23]. The bubble dimensions measured from the photographs are total volume V, horizontal maximum diameter D, height H, and base diameter D_b, as shown in Figure 8(d). The buoyancy expression will be placed in terms of these quantities. The buoyancy of the bubble, excluding the shaded volume V_b of Figure 8(d), is given by

$$(\rho_l - \rho_v)\frac{g}{g_o}(V - V_b)$$

Assuming the shaded volume to be closely approximated by a cylinder (thus neglecting the curvature of the top of the bubble), this can be written as

$$(\rho_l - \rho_v)\frac{g}{g_o}\left(V - \frac{\pi D_b^2 H}{4}\right) \tag{17}$$

The contribution of V_b to the departure force can be expressed in terms of the pressure difference across the interface at the top of the bubble

$$\frac{\pi D_b^2}{4}(P_i - P_o) \tag{18}$$

This pressure difference can be written in terms of the two principal radii of curvature at the top of the bubble

$$(P_i - P_o) = \sigma\left(\frac{1}{R_1} + \frac{1}{R_2}\right)_{\text{top of bubble}} \tag{19}$$

For the bubbles given here, the top portion is spherical, so that R_1 and R_2 can both be approximated by $D/2$. The sum of Equations (18) and (19) with the use of Equation (20) then gives the final expression used to compute the buoyant departure force.

$$F_B = (\rho_l - \rho_v)\frac{g}{g_o}\left(V - \frac{\pi D_b^2 H}{4}\right) + \frac{\pi D_b^2 \sigma}{D} \tag{20}$$

Since the bubble departs by breaking the neck where it is attached to the surface, the surface tension force is given by

$$F_T = \sigma \pi D_b \tag{21}$$

The width of the neck at the bubble base was measured from the photographs. As shown by the values in Figure 8, the width was found to be quite close to the diameter of the drilled site except for the small sites, where the neck appeared somewhat wider than the site. Since the drilled holes were measured directly with a microscope, the precision is higher than the photographic measurement at the bubble base because of distortion by density gradients in the fluid. Hence, it is felt generally more accurate to use the diameter of the drilled site and to compute the surface tension force from

$$F_T = \sigma \pi D_c \tag{22}$$

As shown previously, the volume change with time for the present bubbles was small at the time of departure. This eliminates the possibility of the significance of inertial and drag forces.

A summary of bubble departure dimensions and forces is given in Table I. A plot of buoyancy against surface tension force is given in Figure 9. Within a statistical scatter that seems reasonable for a boiling experiment, the agreement of the two forces is very good. This shows that for the large, slowly growing bubbles studied here, the buoyancy force defined as the integrated vertical pressure force on the bubble is causing departure.

Equilibrium Bubble Shapes

In [24] Bashforth and Adams studied the shapes of drops and bubbles at equilibrium subject to the forces of buoyancy and surface tension. They provide tables of coordinates of the bubble profiles in terms of the parameter

$$\beta = \frac{g(\rho_v - \rho_l)b^2}{g_o \sigma}$$

Since some of the present bubbles fall so close to an equilibrium between surface tension and buoyancy forces at departure, it is of interest to see whether these bubbles compare with the predicted equilibrium shapes. Only the shapes are compared and not the actual bubble sizes as the theoretical results are in terms of dimensionless heights and

radii which involve a scale factor of the radius of curvature b at the top of the bubble. Multiplying by the dimension b to place the curves in dimensional form would not change the relative shapes at a fixed β. The two typical bubbles shown in Figure 10 have values of β of -0.24 and -0.35 and grew, respectively, at mechanically drilled site diameters of 0.0209 and 0.0413 inch. The tables of bubble coordinates in [24] are somewhat incomplete in the range of β of -0.1 to -0.3, and the theoretical curves were supplemented with values given in [25].

The comparisons in Figure 10 reveal that the upper portions of the experimental bubbles are very close to spherical and agree well with the theory. Near the base of the bubbles, the experimental profiles deviate from theory probably because of the constraint imposed by the attachment of the bubble base to the drilled site. The theory on the other hand would allow the bubble base to spread freely over the surface. These considerations reveal an additional factor, other than dynamic forces, present for rapidly growing bubbles, which would account for why the Fritz equation does not always correctly predict the size of bubbles at departure. The Fritz equation is based on theory assuming that the base of the bubble is not constrained, while, depending on the site diameter and geometry, the base of some actual boiling bubbles can remain attached to the site.

CONCLUSIONS

1. Bubble "incipience" is a vague concept. It can be defined in terms of the surface superheat required to make a bubble nucleus grow although the bubble may not detach. Incipience can also be defined as a steady formation of bubbles, thus implying that the bubble must not only begin to grow, but must also be able to reach a size sufficient to cause detachment.

2. The analytical prediction by Hsu [3] appears reasonable for the minimum ΔT to produce incipience based on regular bubble production when a range of cavity sizes is present. The present experimental results show that larger cavities can be active than those indicated by Hsu's model, relating the cavity size and the thermal layer thickness at incipience. The upper limit of active site size is probably due in part to the ability of liquid to fill the site.

3. An incipience criterion was derived for bubble nuclei contained entirely within the thermal layer or extending out of the thermal layer. The theory provided a reasonable lower limit for the experimental ΔT values obtained when bubbles first begin to detach from the surface.

4. In the initial period of bubble growth, the bubble volume is proportional to $\tau^{3/2}$ and is fairly well predictable by the Fritz-Ende equation. Later in the growth period, the volume increases in proportion to τ implying that vapor addition to the bubble may take place through a constant area around the bubble neck.

5. For a given small site, the volumetric growth rate increases approximately as $(\Delta T)^3$ as indicated by many of the growth equations. For a large site the functional relation is not clear, but the growth rate does increase with ΔT.

6. For slowly growing bubbles, the buoyancy and surface tension forces at detachment are in balance. The buoyancy force must include the pressure force deficit caused by the missing bubble area in the contact region at the bubble base.

7. The bubbles detach from the artificial sites studied here by forming a neck which is ruptured some distance above the site and consequently, a vapor nucleus is left behind.

8. Although uniform temperature conditions are not present, the bubbles near their departure from the artificial sites match reasonably well the equilibrium shapes predicted by Bashforth and Adams [24]. Near the bubble base, the constraint imposed by attachment to the artificial site causes some deviation from the predicted shapes.

NOMENCLATURE

A	surface area
a	thickness of specimen containing artificial site
b	radius of curvature at top of bubble
C_1, C_3	dimensionless site geometry constants
D	maximum horizontal bubble diameter
D_b	base diameter of bubble
D_c	diameter of artificial nucleation cavity
F_B	buoyancy force
F_T	surface tension force
g	gravitational acceleration
g_o	conversion constant, 32.2 lb mass-ft/lb force-sec^2
H	bubble height
h	boiling heat transfer coefficient
h_e, h_c	evaporating and condensing heat transfer coefficients for heat transfer to bubble nucleus
k, k_l	thermal conductivity of test specimen or liquid
P_i, P_o	internal and external pressure at top of bubble
q	heat flux
R_c	radius of artificial nucleation cavity
R_1, R_2	principal radii of curvature of bubble
T_o	temperature at insulated surface of test specimen
T_{sat}	saturation temperature of boiling liquid
T_{tl}	mean thermal layer temperature
T_v	temperature of vapor inside bubble
T_w	temperature of boiling surface of test specimen
ΔT	temperature difference, $T_w - T_{sat}$
$(\Delta T)_i$	$(T_w - T_{sat})$ required to form bubbles
V	volume of bubble
V_b	bubble volume lying above area of bubble base
x	distance coordinate from surface
α	thermal diffusivity
β	bubble shape parameter, $(g/g_o)[(\rho_v - \rho_l)b^2/\sigma]$
δ	thermal layer thickness
λ	heat of vaporization
ρ_l, ρ_v	density of liquid or vapor
σ	surface tension of liquid-vapor interface
τ	time

REFERENCES

1. Zuber, N.: "Recent Trends in Boiling Heat Transfer Research. Part I: Nucleate Pool Boiling," Appl. Mech. Rev. vol. 17, no. 9, September, 1964, pp. 663-672.

2. Leppert, G; and C. C. Pitts: "Boiling," Vol. I of Advances in Heat Transfer, edited by T. F. Irvine, Jr. and J. P. Hartnett, Academic Press, New York, 1964, pp. 185-266.
3. Hsu, Y. Y.: "On the Size Range of Active Nucleation Cavities on a Heating Surface," J. Heat Transfer, vol. 84, no. 3, August, 1962, pp. 207-216.
4. Han, C. Y.; and P. Griffith: "The Mechanism of Heat Transfer in Nucleate Pool Boiling. I - Bubble Initiation, Growth and Departure," Intl. J. Heat Mass Transfer, vol. 8, no. 6, June, 1965, pp. 887-904.
5. Griffith, P.; and J. D. Wallis: "The Role of Surface Conditions in Nucleate Boiling," Chem. Eng. Progr. Symposium Ser., vol. 56, no. 30, 1960, pp. 49-63.
6. Rallis, C. J.; and H. H. Jawurek: "The Mechanism of Nucleate Boiling," Paper A/Conf. 28/P/600, Presented at the Third United Nations International Conf. on the Peaceful Uses of Atomic Energy, May, 1964.
7. Strenge, P. H.; A. Orell; and J. W. Westwater: "Microscopic Study of Bubble Growth During Nucleate Boiling," AIChE J. vol. 7, no. 4, December, 1961, pp. 578-583.
8. Yatabe, J. M.; and J. W. Westwater: "Bubble Growth Rates for Ethanol-Water and Ethanol-Isopropanol Mixtures," AIChE Paper No. 7, Presented at the ASME-AIChE 8th Nat'l Heat Transfer Conf., Los Angeles, August, 1965.
9. Bankoff, S. G.: "Entrapment of Gas in the Spreading of a Liquid Over a Rough Surface." AIChE J., vol. 4, no. 1, March, 1958, pp. 24-26.
10. Jeglic, F. A.: "An Analytical Determination of Temperature Oscillations in a Wall Heated by Alternating Current," NASA TN D-1286, July, 1962.
11. Marcus, B. D.; and D. Dropkin: "Measured Temperature Profiles Within the Superheated Boundary Layer Above a Horizontal Surface in Saturated Nucleate Pool Boiling of Water," J. Heat Transfer, vol. 87, no. 3, August, 1965, pp. 333-341.
12. Bergles, A. E.; and W. M. Rohsenow: "The Determination of Forced-Convection Surface-Boiling Heat Transfer," J. Heat Transfer, vol. 86, no. 3, August, 1965, pp. 365-372.
13. Hsu, Y. Y.; and R. W. Graham: "An Analytical and Experimental Study of the Thermal Boundary Layer and Ebullition Cycle in Nucleate Boiling," NASA TN D-594, May, 1961.
14. Grace, T. W.: "The Mechanism of Burnout in Initially Sub-Cooled Forced Convective Systems." PhD Thesis, University of Minnesota, 1963.
15. Wei, C. C.; and G. W. Preckshot: "Photographic Evidence of Bubble Departure from Capillaries During Boiling," Chem. Eng. Sci., vol. 19, October, 1964, pp. 838-839.
16. Zuber, N: "The Dynamics of Vapor Bubbles in Nonuniform Temperature Fields," Intl. J. Heat Mass Transfer, vol. 2, no. 1/2, March, 1961, pp. 83-98.
17. Siegel, R.; and E. G. Keshock: "Effects of Reduced Gravity on Nucleate Boiling Bubble Dynamics in Saturated Water," AIChE J. vol. 10, no. 4, July, 1964, pp. 509-517.
18. Moore, F. D.; and R. B. Mesler: "The Measurement of Rapid Surface Temperature Fluctuations During Nucleate Boiling of Water," AIChE J. vol. 7, no. 4, December, 1961, pp. 620-624.
19. Morin, R.: "Fundamental Studies in Boiling," Paper presented at the 2nd Joint USAEC-Euratom Two Phase Flow Meeting, Germantown, Maryland, April, 1964.
20. Staniszewski, B. E.: "Nucleate Boiling Bubble Growth and Departure," Tech. Rep. No. 16, Massachusetts Inst. Tech. Cambridge, Mass., August, 1959.
21. Fritz, W.; and W. Ende: "Über den Verdampfungsvorgang Nach Kinematographishen Aufnahmen au Dampfblasen," Physik. Zeit., vol. 37, 1936, pp. 391-401.
22. Plessett, M. S.; and S. A. Zwick: "The Growth of Vapor Bubbles in Superheated Liquids," J. Appl. Phys., vol. 25, no. 4, April, 1954, pp. 493-500.
23. Aydelott, J.: NASA-Lewis Research Center, Personal communication.
24. Bashforth, F.; and J. C. Adams: An Attempt to Test the Theories of Capillary Action by Comparing the Theoretical and Measured Forms of Drops of Fluid, Cambridge University Press, 1883.
25. Chun, K. S.: "A Study of Steam Bubbles in Nucleate Boiling," PhD Thesis, Illinois Inst. of Tech., 1956.

TABLE I. - BUBBLE DIMENSIONS AND FORCES AT ONSET OF DEPARTURE

(MECHANICALLY DRILLED SITES)

Bubble diameter, D, in.	Bubble height, H, in.	Diameter of drilled site, D_c, in.	Depth of drilled site, in.	Bubble volume, V, $in.^3$	Buoyancy force, lb	Surface tension force, lb
0.1208	0.181	0.0413	0.030	1.18×10^{-3}	4.74×10^{-5}	4.34×10^{-5}
.1181	.176	↓	↓	1.11	4.55	↓
.1144	.169			1.00	4.25	
.1112	.162			.921	4.06	
.1097	.159			.885	3.98	
.1079	.156			.844	3.87	
.1040	.148			.751	3.65	
.1066	.157	.0304		.796	3.27	3.19
.1035	.146	.0304	↓	.726	3.09	3.19
.0965	.133	.0209	.020	.560	2.26	2.19
.0951	.130	.0209		.540	2.21	2.19
.0829	.106	.0209		.358	1.67	2.19
.0791	.100	.0114		.298	1.17	1.20
.0775	.0968	.0114	↓	.298	1.17	1.20
.0701	.0873	.0076	.010	.207	.790	.798
.0599	.0720	.0076		.123	.515	.798
.0782	.0985	.0075		.278	1.021	.787
.0775	.0970	↓		.270	.997	↓
.0768	.0945			.270	.999	
.0759	.0945			.252	.939	
.0734	.0910			.227	.860	
.0708	.0870			.205	.784	
.0514	.0586	.0038		.0763	.291	.399
.0462	.0508	.0038	↓	.0529	.214	.399

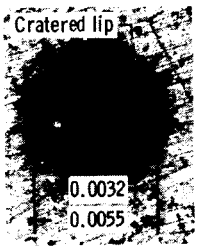

(a) Obtained by electron-beam disintegration; depth, 0.0025 inch. Photographed at 250X.

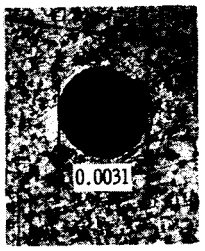

(b) Obtained by mechanical drill; depth, 0.010 inch. Photographed at 290X.

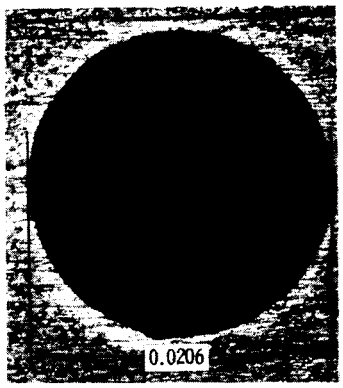

C-66-691

(c) Obtained by mechanical drill; depth, 0.020 inch. Photographed at 150X.

Figure 1. - Photographs of artificial nucleation sites. (All dimensions in inches.)

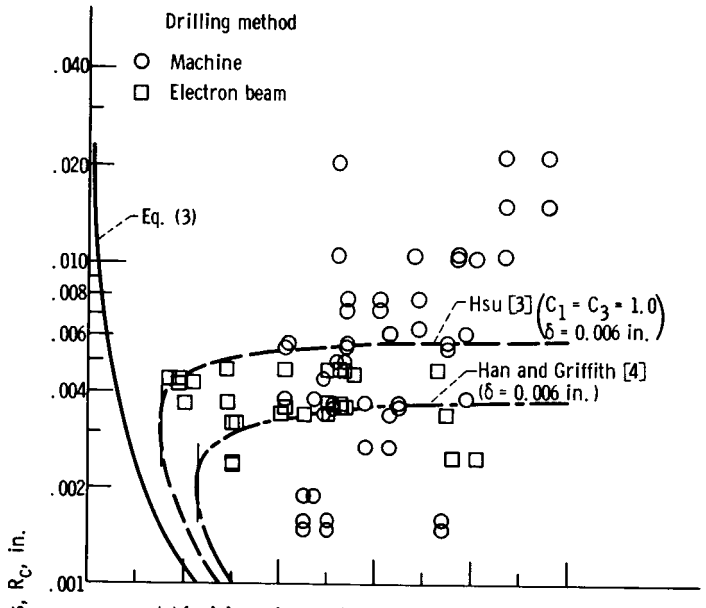

(a) Incipience temperature based on regular site activity.

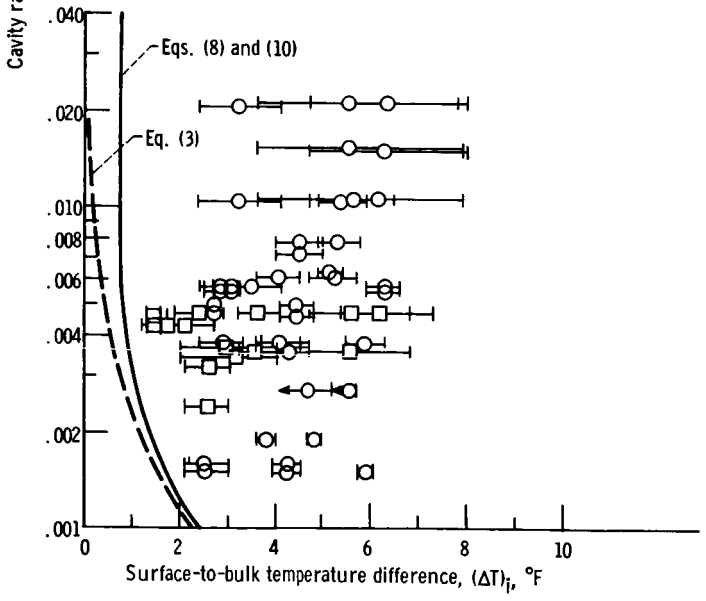

(b) Incipience temperature range from where there are few bursts of bubbles to where bubble detachment ceases.

Figure 2. - Temperature difference required to initiate bubbles from artificial sites.

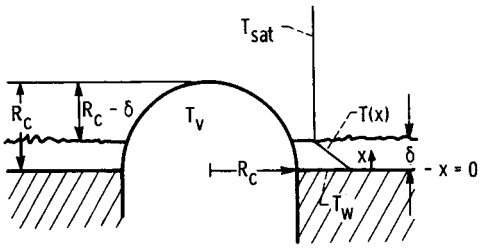

(a) Nucleus extending outside thermal layer.

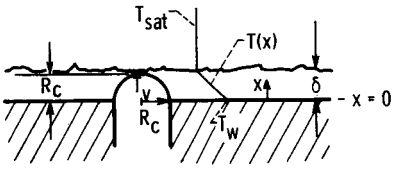

(b) Nucleus contained within thermal layer.

Figure 3. - Criteria for growth of hemispherical bubble nucleus.

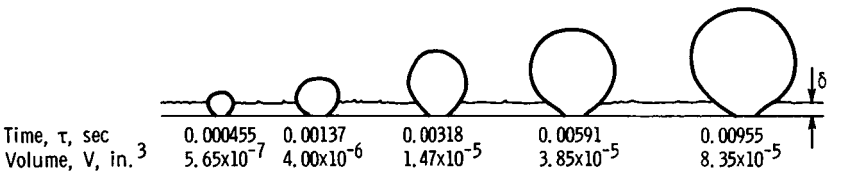

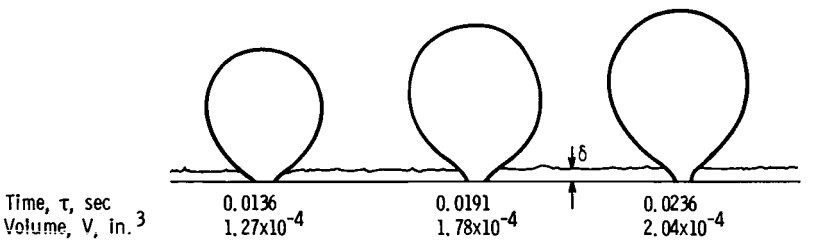

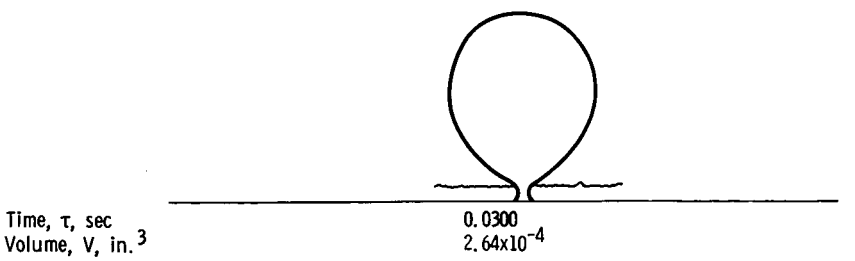

(a) Site diameter, 0.0075 inch.

Figure 4. - Growth profiles of bubbles at artificial site. Temperature difference, ΔT, 8.3° F; thermal layer thickness, δ = 0.006 inch.

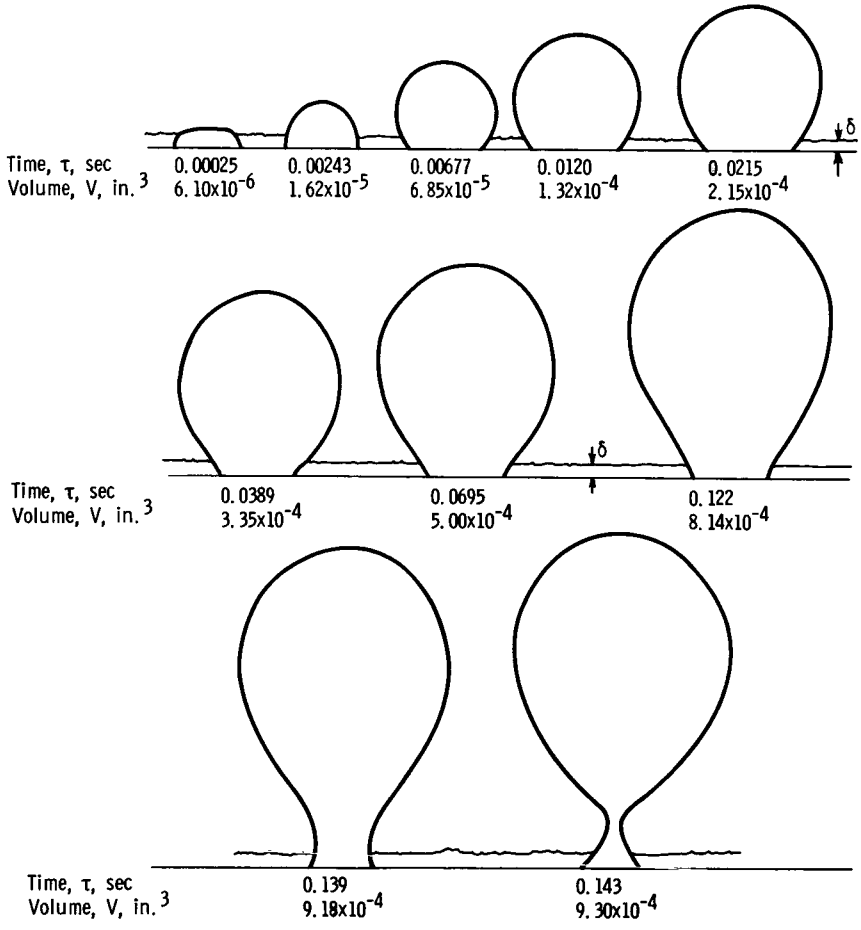

(b) Site diameter, 0.0413 inch.

Figure 4. - Concluded.

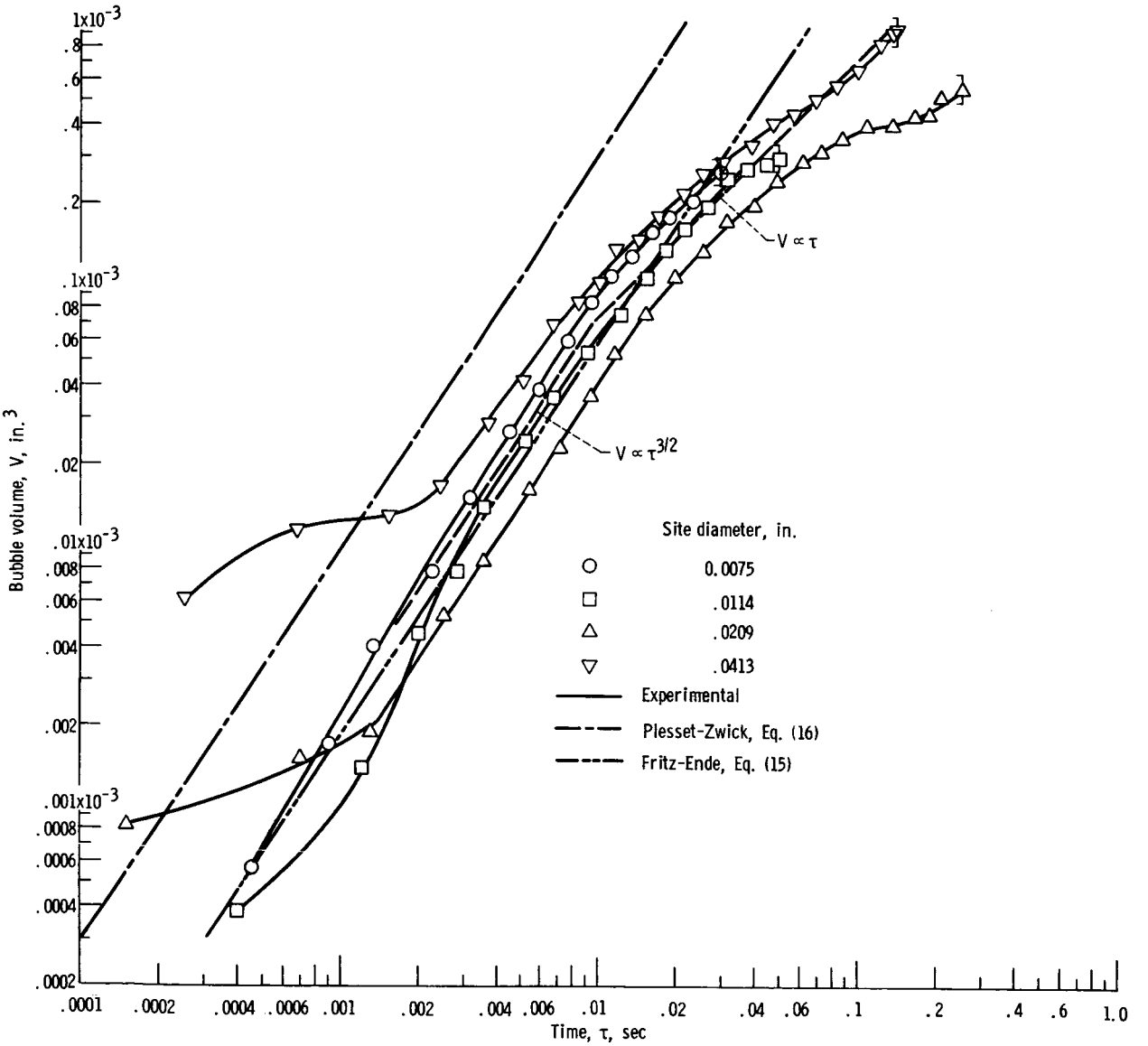

Figure 5. - Effect of nucleation site size on bubble growth rates. Temperature difference, ΔT, 8.3° F.

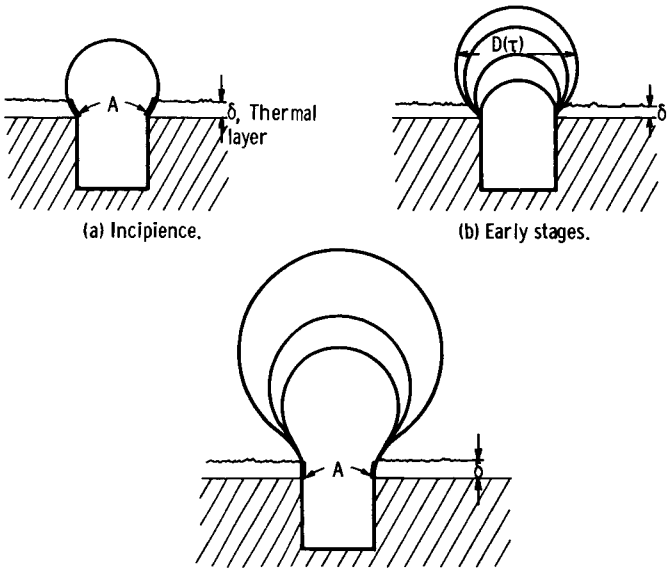

(a) Incipience.

(b) Early stages.

(c) Late stages.

Figure 6. - Stages in growth of bubble from artificial site.

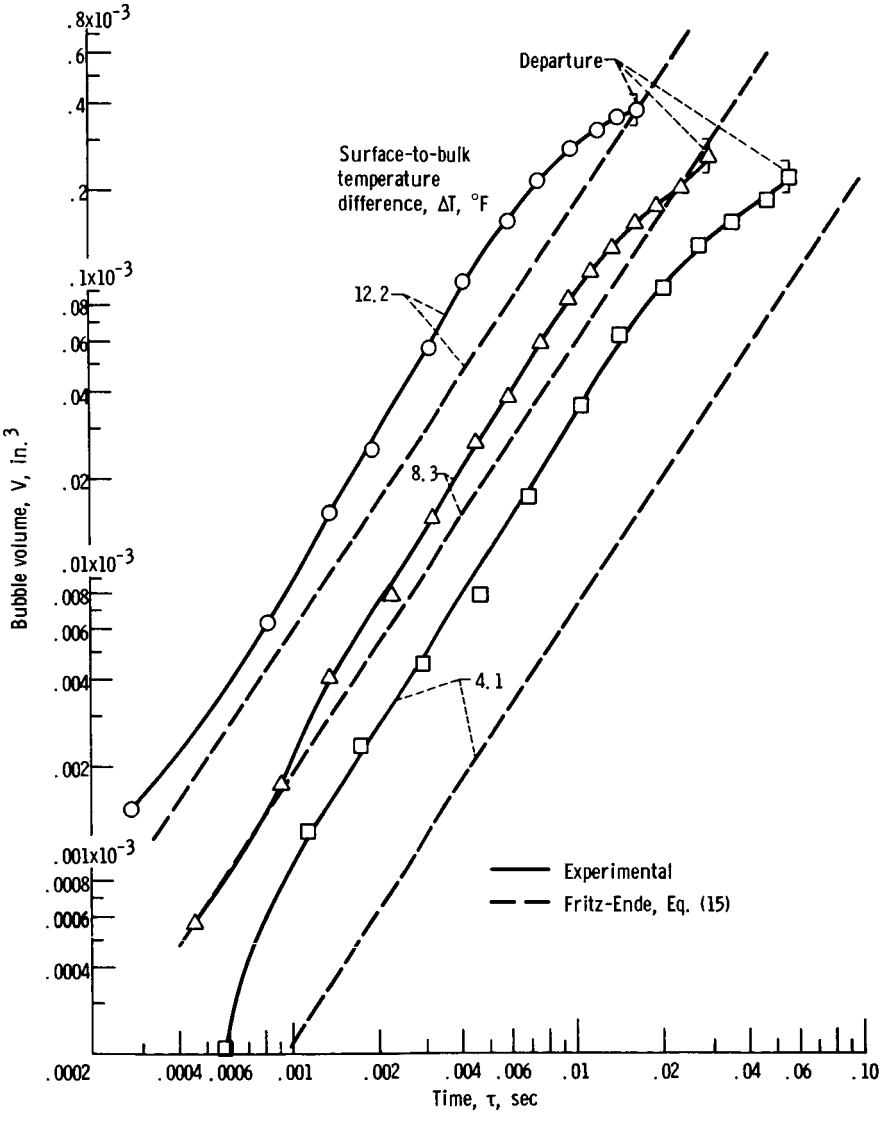

(a) Site diameter, 0.0075 inch.

Figure 7. - Effect of surface-to-bulk temperature difference on bubble growth rates from artificial sites.

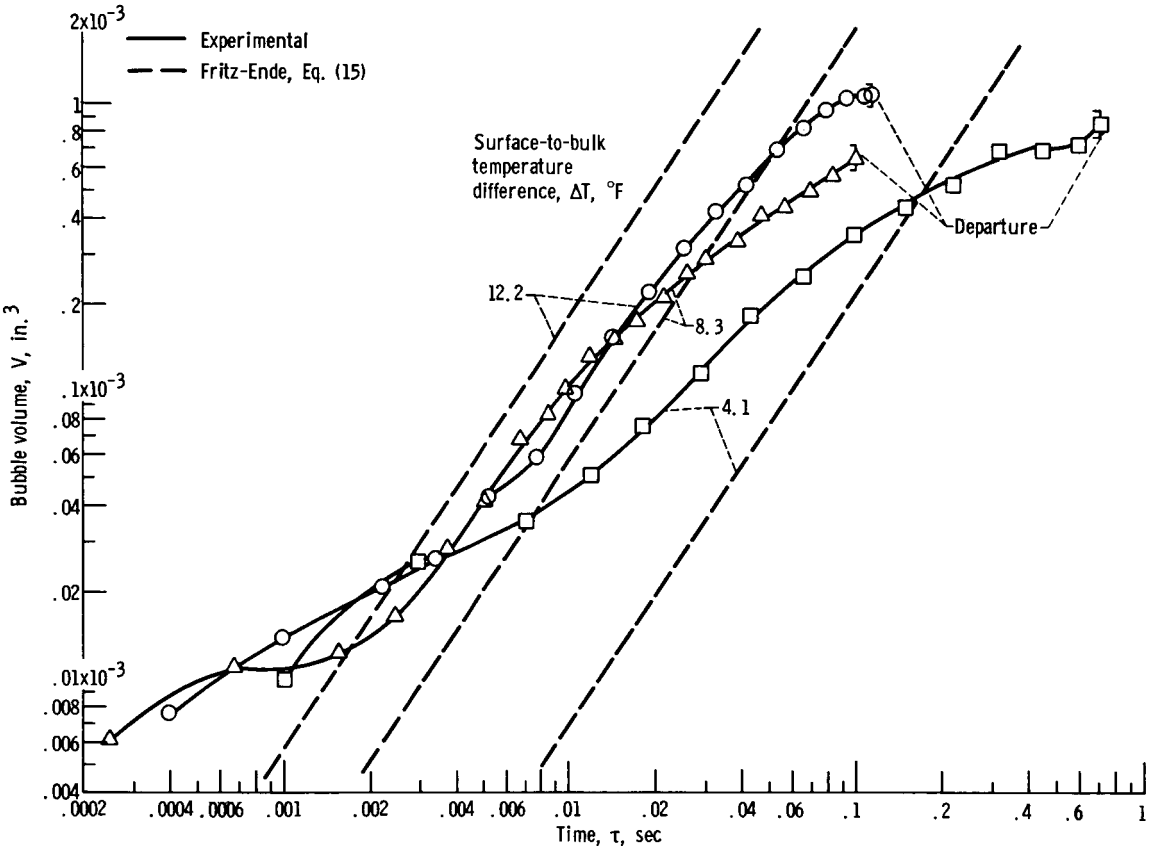

(b) Site diameter, 0.0413 inch.

Figure 7. - Concluded.

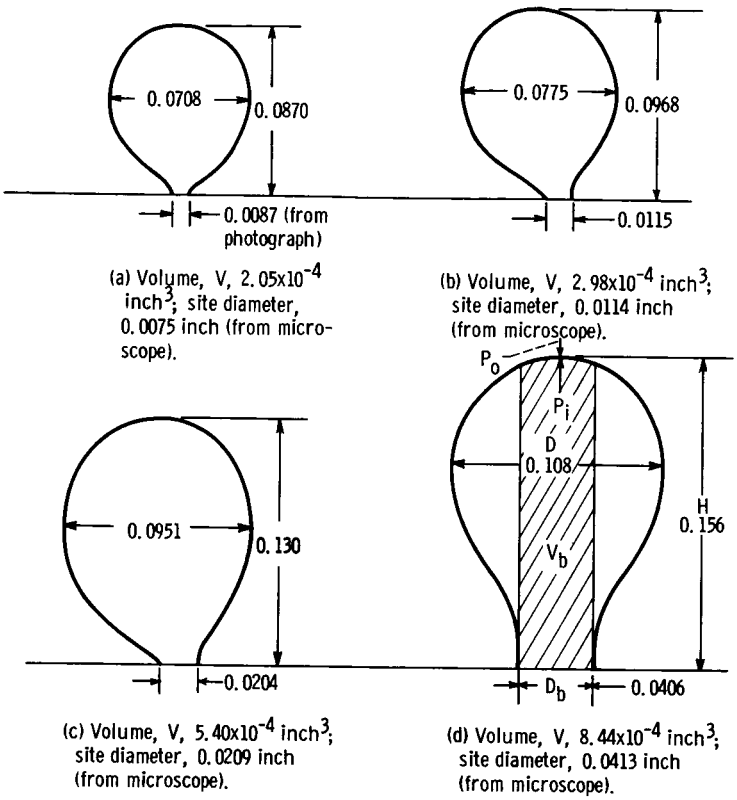

(a) Volume, V, 2.05×10^{-4} $inch^3$; site diameter, 0.0075 inch (from microscope).

(b) Volume, V, 2.98×10^{-4} $inch^3$; site diameter, 0.0114 inch (from microscope).

(c) Volume, V, 5.40×10^{-4} $inch^3$; site diameter, 0.0209 inch (from microscope).

(d) Volume, V, 8.44×10^{-4} $inch^3$; site diameter, 0.0413 inch (from microscope).

Figure 8. - Typical bubble configurations just prior to necking down and departure. Temperature difference, ΔT, 8.3° F. (All dimensions in inches.)

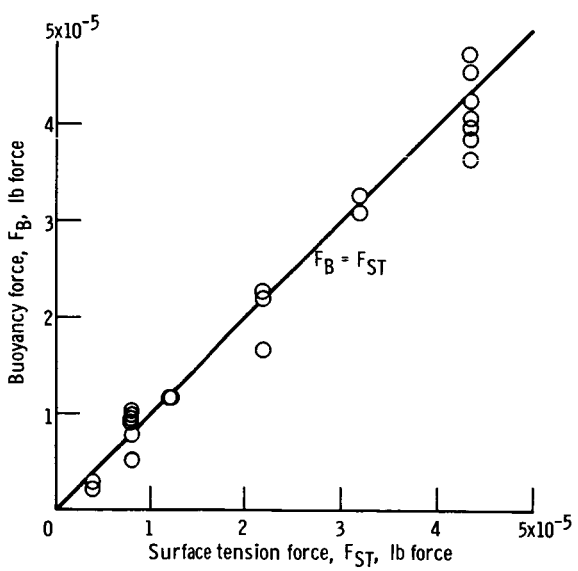

Figure 9. - Comparison of buoyancy and surface tension forces acting on bubbles at onset of departure.

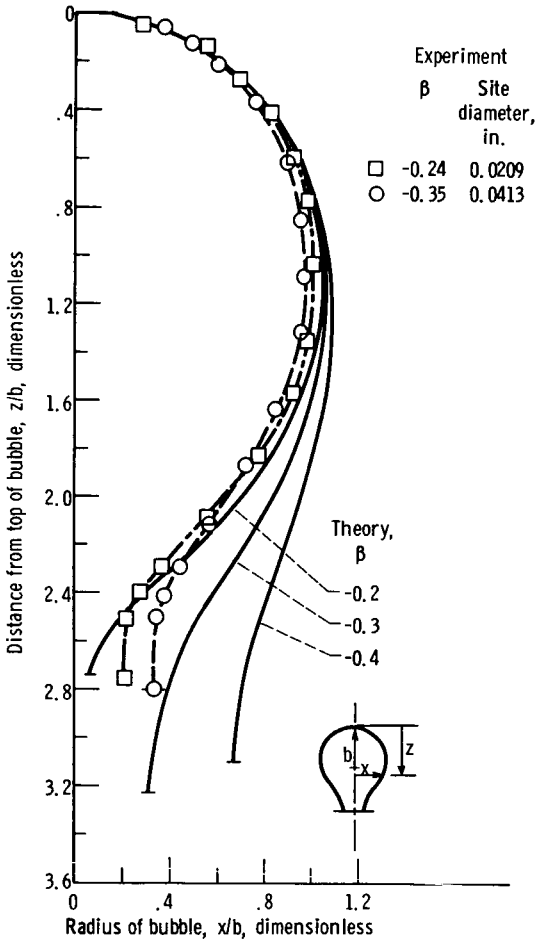

Figure 10. - Comparison of theoretical and experimental bubble profiles at onset of bubble departure when buoyancy and surface tension forces are in equilibrium. Temperature difference, ΔT, 8.3° F.